INTERNATIONAL JOURNAL OF AUTOMOTIVE AND MECHANICAL ENGINEERING
ISSN: 2229-8649 e-ISSN: 2180-1606
VOL. 21, ISSUE 2, 2024, 11332 – 11349
DOI: https://doi.org/10.15282/ijame.21.2.2024.12.0875

RESEARCH ARTICLE

Motorcycle Engine Performance Comparison Between Laser Ignition System and Conventional Ignition System Through Simulation

Tan-Thich Do[1,2], Ly Vinh Dat[2*], Tan-Ngoc Dinh[2]

[1]Department of Mechanical Engineering and Advanced Institute of Manufacturing with High-tech Innovations, National Chung Cheng University, 168, University Rd., Minhsiung Township, 621301, Chiayi, Taiwan
[2]Internal Combustion Engine Department, Faculty of Vehicle and Energy Engineering, Ho Chi Minh City University of Technology and Education, No.1 Vo Van Van Street, Ho Chi Minh City, 720100, Vietnam

ABSTRACT - In many countries, motorcycles have become a primary and popular mode of transportation, driven by increasing demand due to their convenience. However, as fossil fuel sources deplete, there's a pressing need to enhance engine performance, efficiency, fuel economy, and reduce emissions. Improving ignition systems is crucial in achieving these goals. This study compares the performance of the Honda Future FI 125cc engine between a laser ignition system (LIS) and a conventional ignition system (CIS) using simulation. CATIA software was utilized to design the engine's intake manifold, ANSYS Fluent software for simulating and determining the optimal swirl and tumble ratio, and Matlab/Simulink for modeling and simulating engine performance with both LIS and CIS. Detailed discussions and comparisons were made on parameters such as cylinder air mass, ignition energy, engine power and torque, specific fuel consumption (SFC), and mass fraction burned (MFB) between LIS and CIS. Overall, LIS demonstrated superior engine performance compared to CIS. This finding is significant for evaluating the advantages of LIS in motorcycles, especially in the Honda Future FI 125cc engine.

ARTICLE HISTORY
Received : 23rd Jan. 2024
Revised : 26th Apr. 2024
Accepted : 24th May 2024
Published : 20th June 2024

KEYWORDS
Motorcycle engine
Modeling and simulation
Laser ignition system
Conventional ignition system
Engine performance

1.0 INTRODUCTION

Nowadays, motorcycles have become a popular mode of transportation due to their convenience. However, their reliance on gasoline contributes to exhaust emissions and the depletion of fossil fuels. Consequently, enhancing engine performance has become necessary. Up to the present day, notable improvements in engines have been implemented, focusing on components like the intake manifold [1-3] and exhaust manifold [4-5]. Additionally, the integration of advanced technologies has been instrumental in reducing exhaust emissions and improving fuel efficiency [6-9]. Furthermore, significant attention has been directed toward enhancing the ignition system. This aspect plays a pivotal role as the ignition system decisively influences combustion process efficiency and fuel economy. These ongoing efforts in refining both fuel delivery and ignition systems align with the overarching goal of improving the overall performance and environmental impact of motorcycles. The continuous pursuit of advancements in engine technologies reflects a commitment to sustainability and efficiency in the realm of motorized transportation.

The ignition system plays an important role during engine operation. Because the ignition system significantly influences the combustion process efficiency and volumetric efficiency, which affects the engine performance. Recently, the laser ignition system (LIS) has been one of the most noteworthy advancements in ignition technology compared to the conventional ignition system (CIS). LIS was studied and utilized in automobile engines in a laboratory [10-11]. Indeed, Dodd et al. [12] experimented with 4-cylinder engines using the LIS to evaluate the engine performance. The results revealed the advantages of LIS when used in automobile engines. McIntyre et al. [13] experimented with Ricardo Proteus's engine with a high-compression engine under lean burn mode to test the engine emissions. Their findings indicated lower emissions of hydrocarbon products and carbon dioxide. Phuoc et al. [14] investigated the LIS of the constant volume combustion chamber (CVCC) using methane-air mixtures, a method similar to that of Rabii et al. [15]. Their results demonstrated that LIS could be adapted under fuel-rich conditions. Horisawa et al. [16] experimented to investigate the effect of a laser pulse on the combustion process characteristics of fuel-hydrogen injection by utilization of camera techniques to measure the formation of the laser and the laser absorption process. Their results showed that the utilization of LIS has the potential to enhance combustion reactions in the cylinder. Spiglanin et al. [17] investigated the development of combustion process flame evolution in LIS with hydrogen-air mixtures in a CVCC using a camera system to capture videos and analyze them. They concluded that the reaction zones exhibit rapid growth during the initial stages but gradually reduce propagation rate due to the loss of energy of LIS over time. McIntyre et al. [18] developed the laser spark plug, revealing a peak power of the laser over 2 MW. This technology will be used in the future to investigate engine performance under laser beams. Mullett et al. [19] experimented to evaluate the performance of a 4-cylinder engine. Their results showed improved combustion processes in cylinders and stability within the engine speed range of 800 to 1600 revolutions per minute (RPM), along with advanced ignition times at $(16 – 36^0)$. Syage et al. [20] studied the dynamics of flame propagation and measured the minimum laser ignition energy under pulse duration and wavelength.

*CORRESPONDING AUTHOR | Ly Vinh Dat | ✉ datlv@hcmute.edu.vn

Their results showed a minimum laser ignition system energy of 0.21 mJ for hydrogen-air. Ryu et al. [21] carried out experiments involving the LIS with conical cavities and a chamber equipped with jet holes with CVCC. The experiments utilized a mixture of air and methane in the chamber. Their findings indicated that pressure measurements were adjusted to accommodate the quick combustion behavior, which led to a greater maximum pressure and a notable decrease in the overall combustion duration. Dale et al. [22] experimented to evaluate the emissions of an engine using LIS. They concluded that the emissions of hydrocarbons, monoxide, and nitrogen oxides were reduced with the use of LIS. Weinrotter et al. [23] carried out experiments under ultra-lean mixtures of methane, hydrogen, and air to evaluate the combustion process characteristics using LIS in a CVCC. They revealed that hydrogen addition was utilized to enhance combustion process characteristics at the ultra-lean mode. Srivastava et al. [24] experimented to evaluate the formation of laser and the characteristics of LIS in mixtures of hydrogen and air in a CVCC using camera techniques. Kopecek et al. [25] experimented with laser ignition to evaluate the emissions of air-methane mixtures at high-pressure conditions in CVCC under various stoichiometry ratios. They revealed that the emissions were low when using the LIS. Zhai et al. [26] conducted experiments to investigate the effect of LIS on iso-octane and n-heptane using the CVCC. They concluded that the spread of combustion is faster when using n-heptane compared to iso-octane. Meanwhile, Endo et al. [27] experimented to investigate the parameters of LIS and CIS on ignition ability and flame spread speed using the CVCC. Their results indicated that the engine using LIS was superior to CIS. Patil et al. [28] developed an LIS model to evaluate the emissions production of an engine and combustion process characteristics using CVCC under various air-fuel equivalent ratios using numerical simulation methods. They revealed that LIS has the potential compared to CIS, and it can be employed for internal combustion engines in the future. Mohamed et al. [29] conducted experiments to evaluate the minimum ignition energy between LIS and CIS for the CVCC using methane and air mixtures under varying equivalent ratios. Their results indicated that the minimum LIS energy is higher than CIS energy at the same operating conditions. Similarly, Kopecek et al. [30] performed experiments with LIS for the CVCC using methane and air mixtures to evaluate and determine the minimum laser pulse energy (MLPE). They found that the MLPE ranged from 8 to 15 mJ. Similarly, Wang et al. [31] conducted experiments to evaluate the MLPE for the CVCC using oxygen-argon-hydrogen mixtures. They demonstrated that the MLPE of 15 mJ was achieved with hydrogen-oxygen mixtures at stoichiometric proportions.

Recently, Zambalov et al. [32] studied the LIS for the Wankel rotary engine using numerical simulation methods. They revealed that utilizing LIS offers advantages and benefits for the combustion process. The flame was distributed uniformly in the chamber, accelerating the spread of the combustion front across the entire chamber. Kopecek et al. [33] experimented to investigate the LIS on the homogeneous charge compression ignition (HCCI) engine. They concluded that LIS could maintain the HCCI combustion process even at operating conditions of temperatures lower than those typically required. Pal et al. [34] performed an experiment on the effect of laser pulse energy on LIS to evaluate emission characteristics using hydrogen injected into a prototype port-fuel system. They concluded that LIS was adapted to ignite leaner mixtures and significantly reduce NO emissions. Kuang et al. [35] experimented with multi-location laser ignition for a single combustion cylinder. Their results concluded that the engine could reduce the phenomenon of misfires at lean air-fuel mixtures when using the LIS. Liedl et al. [36] conducted experiments to evaluate fuel economy, smoothness, and emissions for Gasoline Direct Injection (GDI) engine with a single-cylinder. They found that when the engine used the LIS, emissions were reduced, fuel was saved, economy was increased, and smoothness was improved compared to CIS. McMillian et al. [37] developed a prototype laser system to evaluate the output efficiency. Their results revealed that the highest output efficiency was achieved at an output coupler (OC) of 80%.

In summary, most studies have focused on the LIS for multi-cylinder engines, especially in automobiles. Additionally, researchers have predominantly studied the characteristics of the combustion process with a CVCC and evaluated emissions using laser sources. Consequently, conducting an engine performance comparison between the LIS and the CIS in motorcycles plays a crucial role and is necessary in assessing the characteristics of single-cylinder internal combustion engines, with a particular focus on the Honda Future FI 125cc engine. This study used computational fluid dynamics (CFD) and numerical simulations to evaluate the engine performance between LIS and CIS. Indeed, ANSYS Fluent software was employed for CFD simulations to determine the optimal swirl ratio and tumble ratio, which significantly impact engine performance. After that, the modeling and simulation of engine performance and ignition system for the Honda Future 125cc engine was built using a Matlab/Simulink environment. Ultimately, the engine performance was evaluated and discussed in detail, including the power engine, torque engine, and specific fuel consumption (SFC). Furthermore, a detailed discussion was conducted on factors including the mass of air in the cylinder, energy of the LIS, energy of the CIS, and mass fraction burned (MFB). This comprehensive analysis holds meaningful implications for evaluating the engine characteristics when utilizing both LIS and CIS in motorcycles. Moreover, this study aimed to establish the theoretical foundation and provide an overview for the subsequent study, which was used to validate the comparison between experimental and theoretical results. On the other hand, before implementing the experiment, modeling and simulation were conducted first to evaluate reliability and cost savings.

2.0 METHODOLOGY

The engine performance was also affected by the shape of the intake manifold of the engine, which significantly influenced the swirl and tumble ratio during the engine operation. Therefore, measurement of the actual dimensions, design, and simulation of the intake manifold are crucial works. Figure 1 depicts the flowchart of the work process with

six significant works in this study. Firstly, the actual dimensions of the engine intake manifold were measured by a special tool. Subsequently, the CATIA software was employed to design the intake manifold shape based on the actual parameters. The ANSYS Fluent software was utilized to simulate CFD to determine the optimal swirl and tumble ratio.

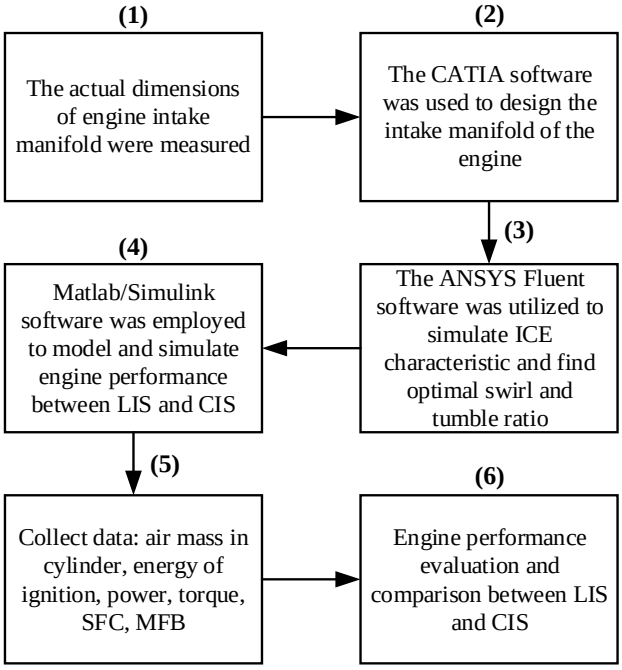

Figure 1. Flowchart related to the work process in this study

In a significant part of this study, the performance of the Honda 125cc engine under LIS and CIS was modeled and simulated in the Matlab/Simulink environment. Consequently, data on mass air in the cylinder, energy of ignition for LIS and CIS, power, torque, SFC, and MFB were recorded. Ultimately, the engine performance between LIS and CIS was evaluated and discussed in detail.

2.1 CFD Simulation to Find the Optimal Swirl and Tumble Ratios

The intake manifold affects the charging process, especially the volumetric efficiency. Therefore, ANSYS Fluent software was used to simulate and find the optimal swirl ratio and tumble ratio in the Honda Future 125cc engine in this study. The results of vertical and horizontal vortex coefficients were used as input parameters to calculate two factors a and m, that affect the combustion process [38].

$$a = 5 + 0.1R_{st}e^{(R_{st}-2)} \quad (1)$$

$$m = 2 + 0.4R_{st}e^{(R_{st}-2)} \quad (2)$$

where: R_{st} represents the summation of turbulent ratios, including swirl (vertical turbulence) and tumble (horizontal turbulence) ratios.

Figure 2 depicts the processes related to engine CFD simulation in the ANSYS Fluent software environment in this study. The actual dimensions of the intake manifold of the Honda Future FI 125cc engine were measured for design in the CATIA software environment, as described in Fig. 2 (a) and (b), respectively. The distribution of mesh and simulation of the engine's dynamics, following the design of the intake manifold, is illustrated in Fig. 2 (c) and (d). After simulating, the optimal swirl and tumble ratio was used to calculate the summation of turbulence.

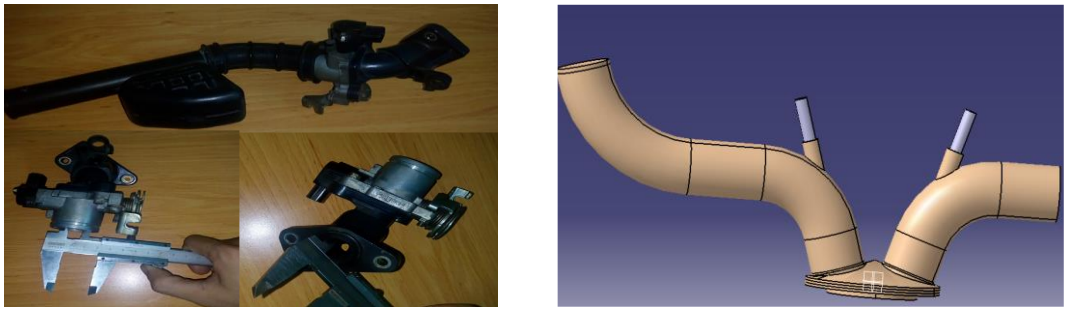

(a) (b)

Figure 2. (a) Measurement of actual dimensions of the Honda 125cc engine intake manifold shape; (b) CATIA software for the design of the intake manifold of an engine;

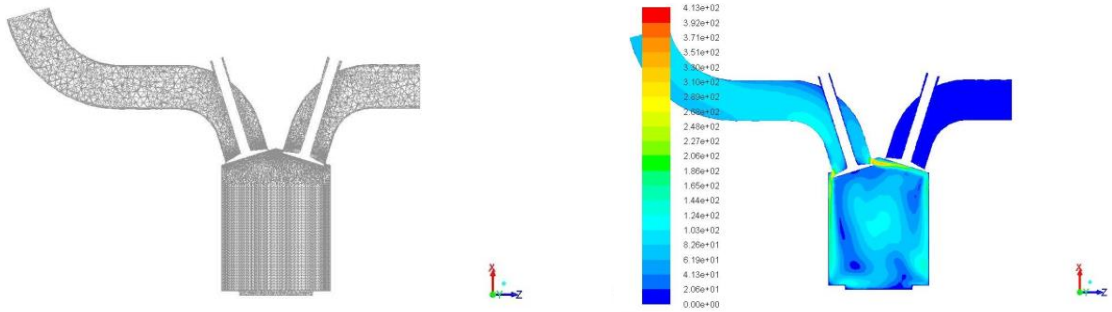

(c) (d)

Figure 2. (cont.) (c) Distribution of the mesh on the ICE shape; and (d) Engine CFD simulation in the ANSYS Fluent software environment, respectively

Figure 3 depicts the relationship between the engine crankshaft angle and the swirl and tumble ratio of the engine. At the power stroke, it can be observed that the optimum ratios for swirl and tumble reached their highest values, approximately 2.7 and 1.3, respectively. Therefore, the summation of turbulents is 4.0.

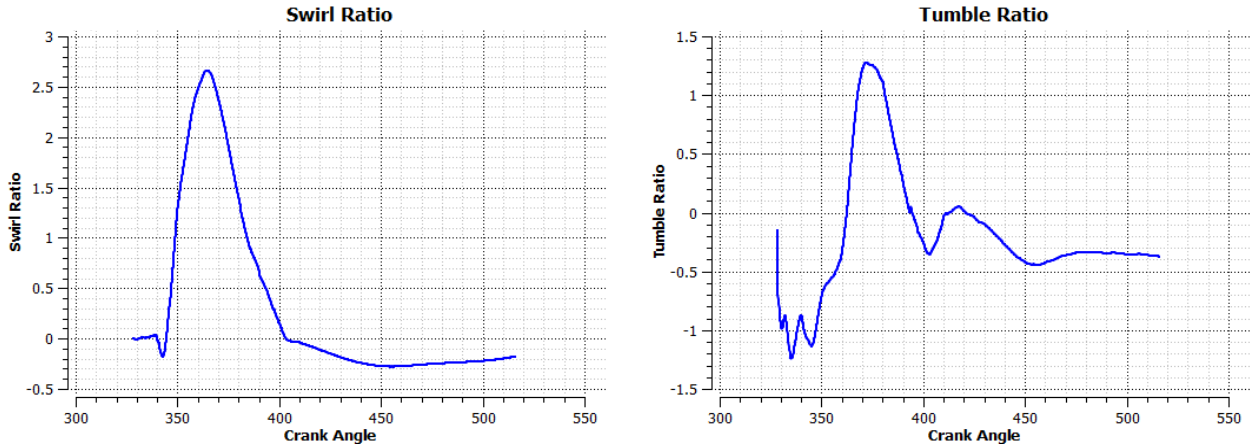

(a) (b)

Figure 3. The relationship between crank angle and swirl ratio (a) and tumble ratio (b), respectively

2.2 Specifications of Honda 125cc Engine, LIS, and CIS

In this study, the engine specifications of Honda Future FI 125cc are listed in Table 1. Additionally, Matlab/Simulink software was utilized to model and simulate the power generation process of the engine when using both CIS and LIS. This is the key main content focus of the study.

Table 1. Honda Future FI 125cc engine specifications

Parameter	Description	Value
C_r	Compression ratio	9.3
D_P	Piston diameter (mm)	52.4
D_{in}	Air intake manifold diameter (mm)	23.2
L	Connecting rod length (mm)	101.5
L_i	Intake valve opening (mm)	0.2
L_e	Exhaust valve opening (mm)	0.2
N_v	Number of valves	2
r	Crankshaft radius (mm)	28.95
V_d	Displacement volume (cc)	125

During engine operation, the engine performance was influenced by many factors, and the ignition system played a significant role in engine power production. The parameters of LIS are crucial for inputting into the Matlab/Simulink software to calculate the engine characteristics. The LIS specifications are described in Table 2.

Table 2. LIS specifications

Parameter	Description	Value
b	Wien's displacement coefficient (m.K)	2.9×10^{-3}
d	Lens diameter (mm)	10
E_B	Energy required to generate a laser (J)	0.4
f	Focal length (mm)	350
P_L	Laser pulse power (kW)	2.67
λ	Laser wavelength (nm)	266

The LIS and CIS are factors that influence the combustion speed, engine performance, and combustion products of the engine. According to ignition theory, a disadvantage of the CIS is that the spark weakens when the engine is running at high speed because it depends on the interrupted current. In contrast, the power of the engine is improved and enhanced by the LIS. The power of the engine meets all operating modes when using the LIS.

For the energy of LIS, energy is not dependent on the interrupted current and growth time of the secondary current. Instead, the energy of LIS relies on the threshold-breaking power density (I_B) and the threshold energy required to generate a laser (E_B).

$$I_B = \frac{1}{\pi}\left(\frac{d_L^2 E_B}{t_L(1.22f)^2}\right) \tag{3}$$

where: d_L, t_L, and f represent the laser beam diameter, laser ignition time, and laser focal length, respectively.

Ultimately, the energy of the laser (E_{LIS}) was calculated as follows:

$$E_{LIS} = 1.94 \times 10^4 \sqrt{I_B} \tag{4}$$

In this study, to compare the characteristics of the engine between using LIS and CIS, the parameters for the conventional ignition system are listed in Table 3.

Table 3. CIS specifications

Parameter	Description	Value
C_1	Primary coils capacitance (F)	0.7×10^{-6}
C_2	Secondary coils capacitance (F)	1.0×10^{-10}
E_C	Energy of capacitive ignition (mJ)	100
K_i	Ignition reserve coefficient	1.5
L_1	Primary coils inductance (H)	1.48×10^{-3}
N_1	Number of primary windings (circles)	350
N_2	Number of secondary windings (circles)	19000
R_1	Primary windings resistance (Ω)	0.6
t_1	Ignition factor coefficients (H. Ω^{-1})	0.0010
U_1	Primary winding voltage (V)	12
η_{CIS}	CIS ignition performance	0.8

The energy of the CIS was dependent on many factors, particularly the power-off process at the primary winding and the growth time of the secondary current, referred to as the "dwell angle." The interrupted current can be determined as follows [39]:

$$I_{int} = \frac{U_1}{R_1}\left(1 - e^{-\frac{t_d}{t_1}}\right) \tag{5}$$

where: U_1, R_1, t_d, and t_1 represent the voltage of the battery, resistance of the primary winding, ignition time, and ignition factor coefficients, respectively.

The energy of the CIS (E_{CIS}) in the Honda Future FI 125cc engine includes both factors of ignition energy of capacitive (E_C) and inductive (E_I). The energy of the inductive depends on the inductance of the primary coil (L_1) and interrupted current (I_{int}). The energy of CIS can be calculated using the following equation:

$$E_{CIS} = E_I + E_C = \frac{1}{2}L_1 I_{int\_max}^2 \left(1 - e^{-\frac{t_d}{t_1}}\right)^2 + E_C \tag{6}$$

2.3 *Modeling and Simulation of the Engine Performance*

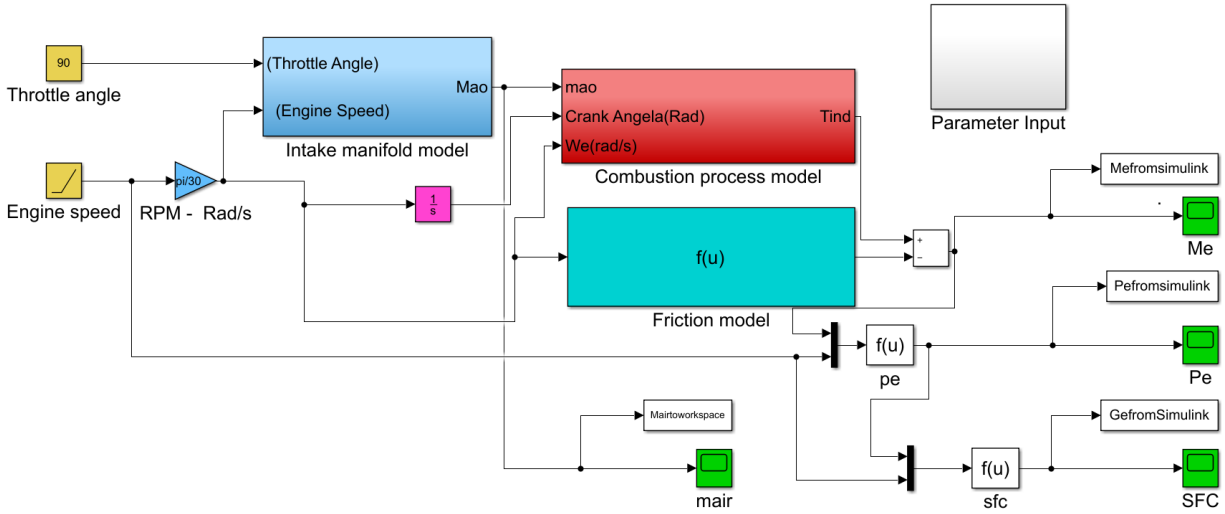

Figure 4. Modeling the Honda Future FI engine performance with LIS and CIS by using Matlab/Simulink

Figure 4 illustrates the model of the Honda Future FI 125cc engine performance with LIS and CIS, constructed using Matlab/Simulink. It encompasses subsystem blocks, including input parameters, intake manifold model, combustion process model, and friction model. Additionally, the model displays results such as mass air in the cylinder, engine power, engine torque, SFC, and MFB.

2.4 *Modeling and Simulating Intake Manifold*

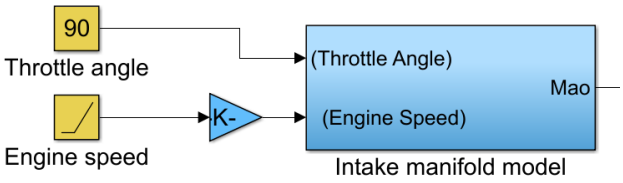

Figure 5. Modeling the intake manifold for the Honda Future FI 125cc engine

Figure 5 depicts the intake manifold model for the Honda Future FI 125cc engine, including input parameters like throttle angle and speed of the engine. The output parameter is the mass flow rate of air entering the cylinder. The relationship between the area of the throttle valve and the throttle angle, along with the dimensions of the throttle valve, was calculated as follows:

$$A(\varphi) = -\frac{dD}{2}\left[1-\left(\frac{d}{D}\right)^2\right]^{\frac{1}{2}} + \frac{dD}{2}\left[1-\left(\frac{d}{D}\frac{cos(\alpha_0)}{cos(\alpha_0+\alpha)}\right)^2\right]^{\frac{1}{2}} + \frac{D^2}{2}sin^{-1}\left\{\left[1-\left(\frac{d}{D}\right)^2\right]^{\frac{1}{2}}\right\} - \frac{D^2}{2}\frac{cos(\alpha_0)}{cos(\alpha_0+\alpha)}sin^{-1}\left\{\left[1-\left(\frac{d}{D}\frac{cos(\alpha_0)}{cos(\alpha_0+\alpha)}\right)^2\right]^{\frac{1}{2}}\right\} \quad (7)$$

where: d, D, α, α_0 represent the throttle shaft diameter (m), the diameter of the throttle valve bore (m), the throttle valve angle (deg), and the initial angle of the throttle valve (deg), respectively.

During engine operation, the mass flow rate of air before the throttle valve depends on variables such as the area of the throttle valve, ambient pressure, and coefficient of discharge. The airflow rate before and after the throttle valve was determined following the equation based on Moskwa's thesis [40]:

$$\dot{m}_{ai} = C_d A(\varphi)\frac{P_0}{\sqrt{RT_0}}\left(\frac{P_t}{P_0}\right)^{\frac{1}{k}}\left\{\frac{2k}{k-1}\left[1-\left(\frac{P_t}{P_0}\right)^{\frac{k-1}{k}}\right]\right\}^{\frac{1}{2}} \quad (8)$$

where: C_d is the coefficient of discharge, $A(\varphi)$is the throttle valve area, P_0 is the upstream pressure of air, P_t is the pressure of throat throttle (occurred at a minimum area at the throttle valve), k is a specific heat of air ratio, T_0 is the air upstream temperature, and R is the universal gas constant. After the mass flow rate of air passes the component of the throttle valve, the air mass flow rate output can be determined as follows:

$$\dot{m}_{ao} = \frac{P_m V_d}{\pi R T_m} \omega_e \eta_v \tag{9}$$

where: P_m, V_d, T_m, ω_e, and η_v denote the air pressure at the intake manifold, displacement volume, air temperature, engine angular velocity, and volumetric efficiency, respectively.

Figure 6 shows the subsystem of the model of the airflow rate passing through the throttle valve, encompassing the entry of air into the throttle valve as depicted in Figure 6 (a). The throttle angle influences the pivot throttle angle, valve diameter, and rotation angle. The air mass flow rate is determined after passing through the component of the throttle valve, as shown in Figure 6 (b).

After the air passes through the component of the throttle valve, the air combines with fuel to produce the mixture. Figure 7 illustrates the model of the intake manifold for the Honda Future 125cc engine, encompassing the modeling of airflow passing through the component of the throttle valve and the air mass flow rate entering the cylinder.

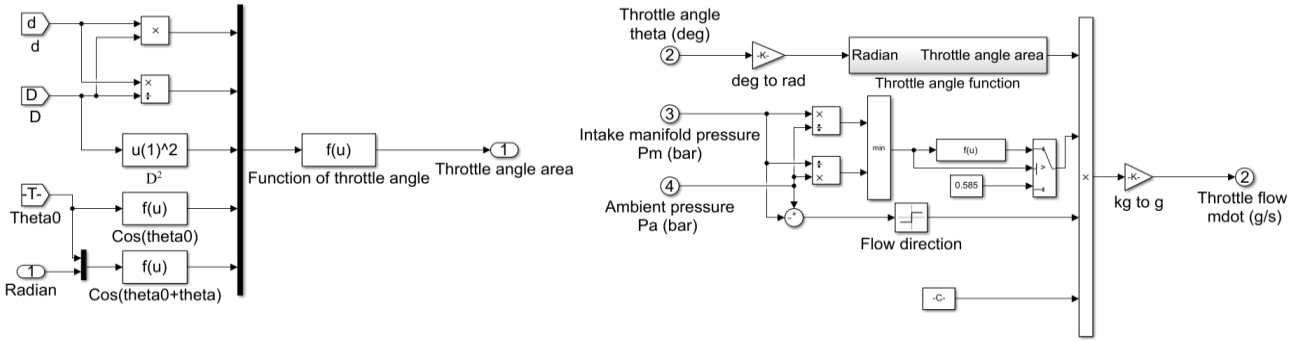

(a) (b)

Figure 6. (a) Subsystem of the air passing through the component of throttle valve; (b) Calculation of air flow rate passing through the component of throttle valve

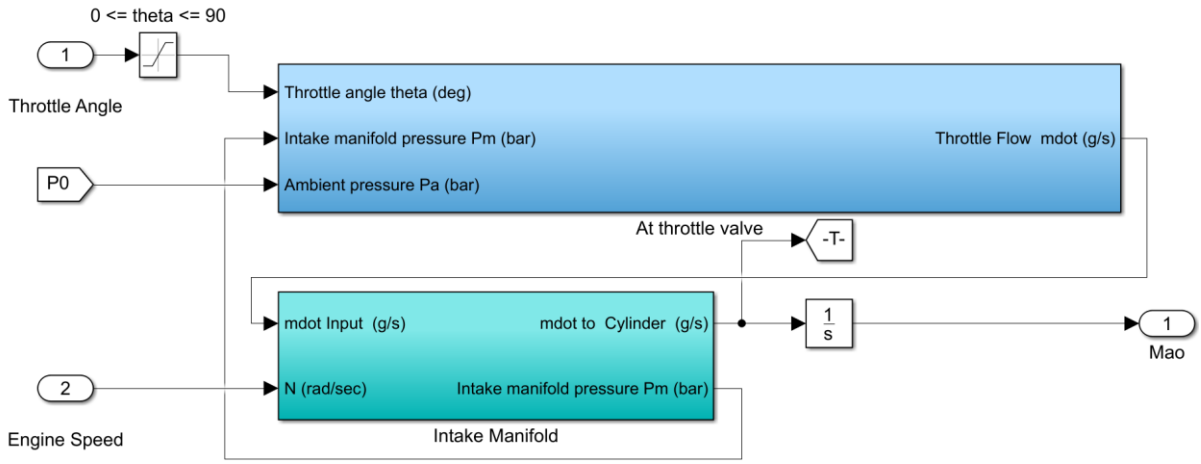

Figure 7. Subsystem block in intake manifold model for Honda Future 125cc engine

2.5 Modeling and Simulating the Process of Combustion

The mixture entering the cylinder undergoes the combustion process to produce power and torque. Figure 8 shows the combustion process model, with the output parameter being engine torque. In this subsystem, the swirl and tumble ratio were considered. ANSYS Fluent was employed to simulate CFD to refine the optimal intake affect coefficient as determined previously. Additionally, the heat transfer and heat release, y-effect, pressure, and displaced volume of the cylinder during the combustion process were calculated.

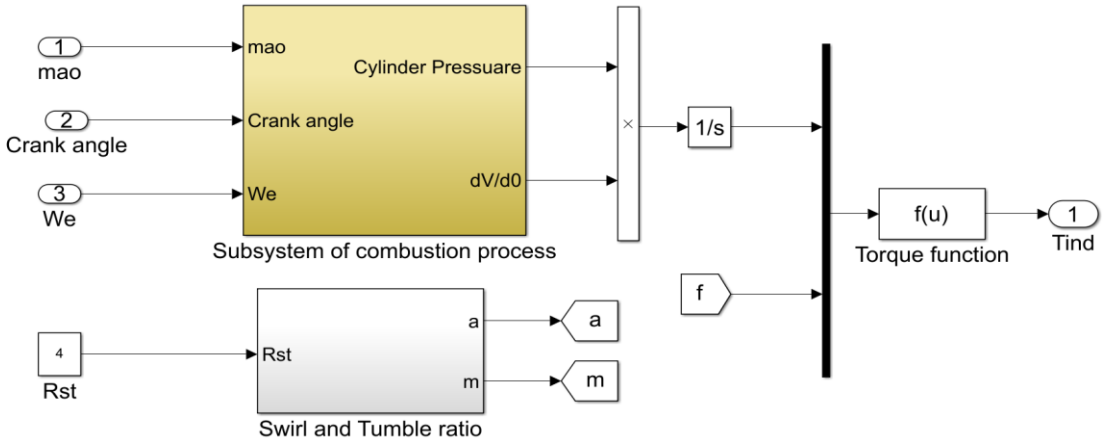

Figure 8. Model of the combustion process and work done

To calculate the heat release rate, the factor parameter y, representing the rate of MFB (x_b), was determined through charge motion, which includes swirl and tumble coefficients (a, m), and crankshaft angle (φ). This calculation was based on the Wiebe fire function:

$$y = \frac{dx_b}{d\varphi} = a\frac{m+1}{\varphi_d}\left(\frac{\varphi-\varphi_0}{\Delta\varphi}\right)^m e^{-a\left(\frac{\varphi-\varphi_0}{\varphi_d}\right)^{m+1}} \tag{10}$$

where: φ_0, and φ_d denote the advanced ignition angle and total combustion time, respectively.

The mass fraction burned (x_b) can be determined as follows:

$$x_b = 1 - e^{-\left(\frac{\varphi-\varphi_0}{\varphi_d}\right)^{m+1}} \tag{11}$$

During the process of combustion, the relationship between heat release (Q_{hr}) and crankshaft angle can be determined through the fuel heating value (Q_{HV}) and the weight of fuel per cycle (m_f), and factor parameter y following the equation (12). Also, Figure 9 below depicts the heat release rate model during the process of combustion.

$$\frac{dQ_{hr}}{d\varphi} = yQ_{HV}m_f \tag{12}$$

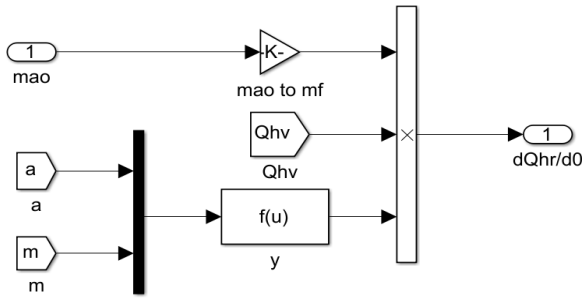

Figure 9. The model of heat rate

In addition, the rate of heat transfer was determined based on the convective heat transfer coefficient h ($m^{-2}K^{-1}W$), the area of the combustion chamber A_c (m^2), combustion wall temperature T_w (K), and temperature during charging T (K):

$$\frac{dQ_{ht}}{d\varphi} = hA_c(T - T_w) \tag{13}$$

The heat transfer coefficient depends on the mixture combustion temperature T_g (K), pressure in cylinder P (bar), and engine speed N (RPM). The heat transfer coefficient was obtained by using the following equation (14). Ultimately, the heat transfer rate is shown in Fig.10 below, which was modeled through some input parameters.

$$h = 1.92 \times 10^6 P^{0.635} T_g^{-1.45}\left(0.119\frac{N}{30} + 1.4\right)^{0.052} \tag{14}$$

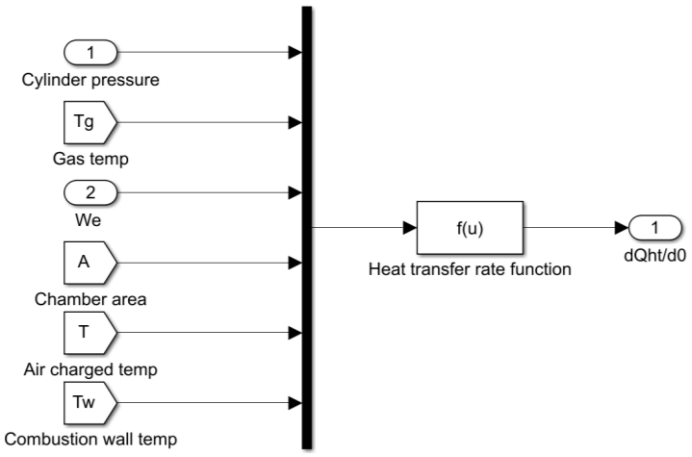

Figure 10. The model of heat transfer rate in the combustion process

After the mixture was burned, the engine work was produced and represented by the pressure. The relationship between instantaneous pressure in the cylinder and crank angle ($dp/d\varphi$) was calculated based on heat release, heat transfer, and volume of the cylinder of an engine. The instantaneous pressure in the cylinder can be determined by:

$$\frac{dp}{d\varphi} = -\gamma \frac{p}{V}\frac{dV}{d\varphi} + \frac{\gamma - 1}{V}\left(\frac{dQ_{ht}}{d\varphi} - \frac{dQ_{hr}}{d\varphi}\right) \tag{15}$$

In addition, the instantaneous volume of the cylinder is a function of crank angle φ (deg), engine displacement volume V_d (m^3), engine compression ratio C_r, crankshaft radius of the engine r (m), and connecting rod length L (m). The relationship was calculated as follows:

$$V = \frac{V_d}{2}\left(\frac{2}{C_r - 1} + 1 - cos(\varphi) + \frac{r}{4L}(1 - cos(2\varphi))\right) \tag{16}$$

The instantaneous rate of volume change in the cylinder was determined by:

$$\frac{dV}{d\varphi} = \frac{V_d}{2}\left(sin(\varphi) + \frac{r}{2L}sin(2\varphi)\right) \tag{17}$$

The energy of ignition affected the engine performance. The energy of CIS included both the energy of inductive ignition and the energy of capacitive ignition. The energy of inductive ignition depended on the ignition time, as mentioned in equation (6). The energy of capacitive ignition depended on the parameters of the ignition system and was a key factor. The energy of capacitive ignition was calculated as follows:

$$E_C = \frac{CU_{iv}^2}{2} = \frac{C}{2}\left(\frac{U_2}{K_i}\right)^2 \tag{18}$$

where C is the capacitive in the primary coils and secondary coils (F), U_{iv} is the ignition voltage at the spark plug (V), U_2 is the voltage of the secondary coils (V), and K_i is the ignition reserve coefficient.

Before the high voltage occurred at the spark plug, energy had been accumulated in the primary coils in the form of a magnetic field. The accumulated energy was defined as follows:

$$E_{cc} = \frac{L_1 I_{int\_max}^2}{2} = \frac{L_1}{2}\left(\frac{U_1}{R_1}\right)^2 \tag{19}$$

where L_1, U_1, and R_1 denote the primary coil inductance (H), primary windings voltage (V), and primary windings resistance (Ω), respectively.

The accumulated energy included the capacitance of both the primary and secondary coils. This accumulated energy led to heat generation in the ignition coils. Therefore, the accumulated energy was considered the CIS ignition performance, as follows:

$$\eta_{CIS}\frac{L_1}{2}\left(\frac{U_1}{R_1}\right)^2 = \frac{C_1 U_1^2}{2} + \frac{C_2 U_2^2}{2} \tag{20}$$

where η_{CIS}, U_2, C_1, and C_2 represent the CIS ignition performance, the voltage of the secondary coils (V), the primary coils capacitance (F), and the secondary coils capacitance (F), respectively.

On the other hand, there exists a relationship between the voltage of the primary and secondary coils and the number of primary coils (N_1) and the number of secondary coils (N_2). This relationship is shown below:

$$\frac{U_1}{U_2} = \frac{N_1}{N_2} \tag{21}$$

Therefore, equation (20) was arranged as follows:

$$\eta_{CIS} \frac{L_1}{2} \left(\frac{U_1}{R_1}\right)^2 = \frac{C_1}{2} \left(\frac{U_2 N_1}{N_2}\right)^2 + \frac{C_2 U_2^2}{2} \tag{22}$$

Consequently, the voltage of secondary coils was determined by equation (23):

$$U_2 = \frac{U_1}{R_1} \sqrt{\frac{L_1}{C_1 \left(\frac{N_1}{N_2}\right)^2 + C_2} \eta_{CIS}} \tag{23}$$

Substituting the values from Table 3 into equation (23), the voltage of the secondary coils is calculated to be 37.45 kV. The capacitive in the primary coils and secondary coils (F) was determined as follows:

$$C = C_1 \left(\frac{N_1}{N_2}\right)^2 + C_2 \tag{24}$$

The energy of capacitive ignition was calculated from equation (19) to be 100 mJ. The energy of CIS, including the energy of capacitive ignition and inductive ignition was calculated by:

$$E_{CIS} = E_I + E_C = \frac{1}{2} L_1 I_{int\_max}^2 \left(1 - e^{-\frac{t_d}{t_1}}\right)^2 + 100 \tag{25}$$

In the subsystem of the heat transfer rate function, when ignition occurs and starts to burn the mixture in the cylinder, the spectral distribution varies as a function of temperature. The relationship between laser wavelength and the temperature of the air charged in the cylinder is described by the following equation, commonly referred to as Wien's displacement law [41]:

$$\lambda = \frac{b}{T} \tag{26}$$

The laser energy depends on many factors, including the threshold energy required to generate a laser, focal length, wavelength, lens diameter, and ignition time of the laser. The specifications and energy of the laser were mentioned in section 2.2. Ultimately, the energy of the ignition systems was modeled and calculated for both CIS and LIS, as illustrated in Figure 11 (a) and (b), respectively.

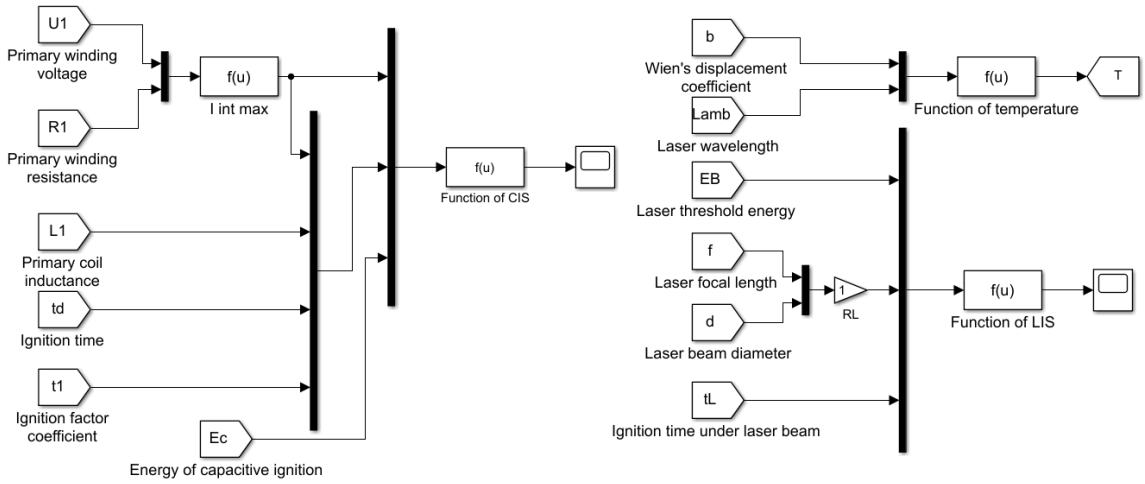

(a) (b)

Figure 11. (a) Modeling of the CIS energy; (b) Modeling of the LIS energy

Figure 12 illustrates the model of the combustion process, encompassing the subsystems of heat release rate and heat transfer rate. Additionally, it includes the functions of instantaneous volume in the cylinder, instantaneous volume change rate in the cylinder, and instantaneous pressure in the cylinder.

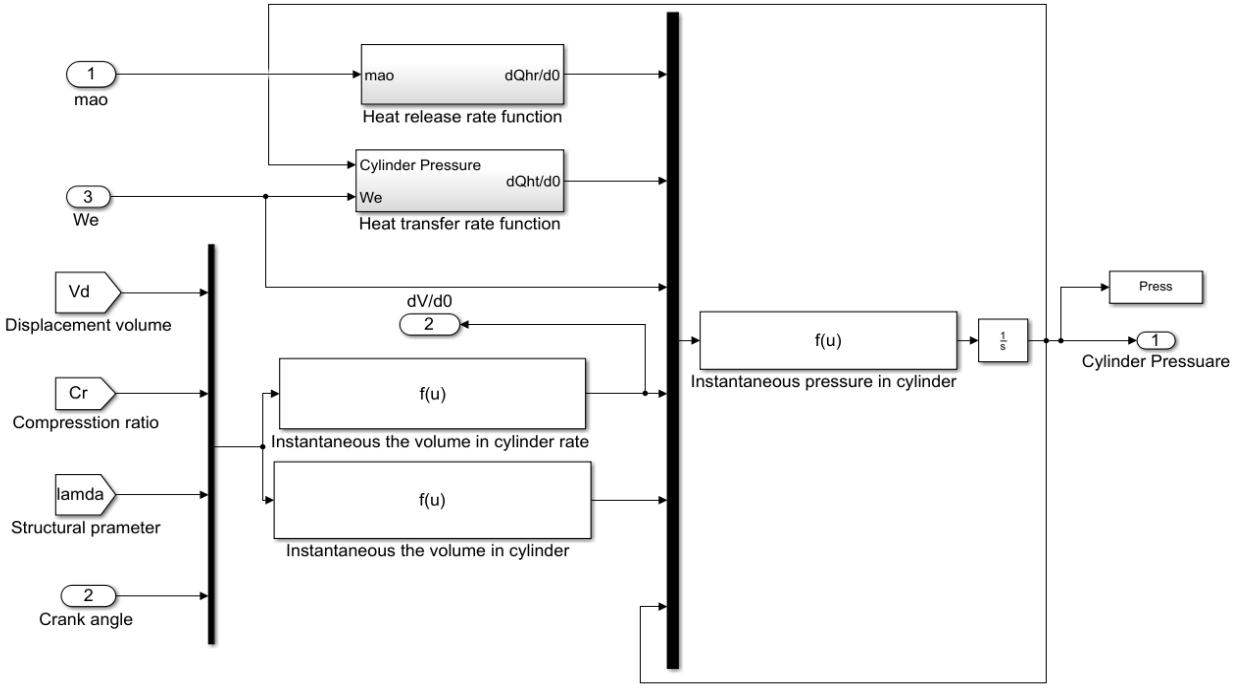

Figure 12. Modeling of pressure in the cylinder, which is related to the engine combustion process

2.6 Modeling and Simulating Engine Friction Loss Model

The engine friction loss occurs during engine operation. Theoretically, a lower engine friction value is preferable. The total engine friction depends on the coefficient of dimension C_D, pumping loss P_P (MPa/RPM^2), engine speed N (RPM), and lubrication oil viscosity V_L (MPa). Therefore, the friction torque was determined as follows [42]:

$$T_{fr} = \frac{C_D(P_P N^2 + V_L)}{4\pi} \tag{27}$$

2.7 Modeling and Simulating the Work Done by the Engine

The indicated engine torque T_{ind} (N.m) depends on the torque function T_F (N.m/g) and air mass charged in the cylinder M_{ac} (g). It can be calculated as follows:

$$T_{ind} = T_F M_{ac} \tag{28}$$

The torque function represents the change in the engine torque during engine operation. It depends on the pressure at the intake manifold P_m (bar) and angular velocity of the engine ω_e (rad/s):

$$T_F = 2.61\left[44.8 - 3.723\left(\frac{P_m}{1.013}\right)^{-0.258} - 9.77\omega_e^{-0.088}\right] \tag{29}$$

The brake torque T_{br} (N.m) was determined based on the indicated engine torque T_{ind} (N.m) and friction torque T_{fr} (N.m) as follows:

$$T_{br} = T_{ind} - T_{fr} \tag{30}$$

Ultimately, the engine power output P_{br} (W) can be expressed as follows:

$$P_{br} = T_{ind}\omega_e \tag{31}$$

In summary, the engine performance between LIS and CIS was modeled and simulated using Matlab/Simulink software. Parameters such as mass of air in the cylinder, energy of ignition, engine power, torque, specific fuel consumption, and mass fraction burned were calculated and determined. These aspects will be discussed in detail in the results and discussion part.

3.0 RESULTS AND DISCUSSION

3.1 Comparision the Air Mass in a Cylinder between Using LIS and CIS

Figure 13 depicts the relationship between the engine speed and the air mass in the cylinder for both the LIS and CIS. It was evident that when the speed of the engine increased from the initial start to 9000 RPM, the mass of air in the cylinder gradually increased from 3.3 to 6.0 g.s^{-1}. This indicates that as the throttle angle valve was opened further, a greater air mass entered the cylinder. In addition, the mass of air in the cylinder was also addressed and discussed in previous research by Colin et al. [43].

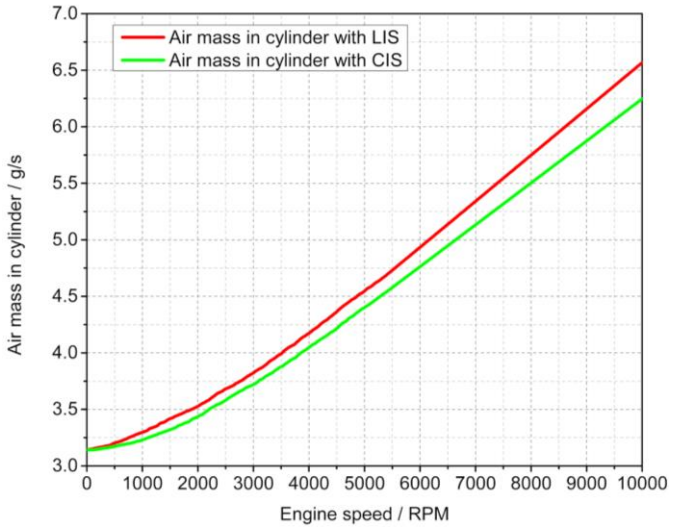

Figure 13. Air mass in the cylinder for LIS and CIS

The air mass in the cylinder for the LIS is higher than that for the CIS. This difference can be attributed to the more effective expulsion of residuals and products in the LIS, resulting in a superior intake process compared to the CIS.

3.2 Energy of LIS and CIS

Figure 14 depicts the evolution of the energy for both LIS and CIS. It can be observed that the energy of CIS gradually increased, reaching saturation at approximately 100.08 mJ after 0.003 s. The energy of CIS encompasses the capacitance and inductance. As the engine speed increased, the energy of CIS could not adapt because it was insufficient, resulting in a low revolution of the secondary current. Obviously, as the engine speed increased, the engine with CIS could misfire due to insufficient energy. To ensure sufficient energy for CIS, it should have enough time to reach saturation. This time is called the "dwell-ignition" time. In fact, a lower dwell-ignition time value is preferable.

For LIS, its energy does not depend on the interrupting current as well as the growth of the secondary current. The energy of LIS depends on the break threshold, power density threshold, and energy threshold used to generate the laser beam. At 0.001 ms, the energy of LIS reached a maximum of approximately 5100 mJ, surpassing the energy of CIS of 100 mJ. The ignition time was short, with no time lag. However, the energy of LIS gradually decreased due to photon energy loss during radiation expansion. The transition of laser energy from a high energy level to a low energy level resulted in losses of energy. This phenomenon was also discussed similarly in previous works by Trawniczek, Franz et al. [44] and [45]. In terms of spark sensitivity, the LIS demonstrated a prompt response without delay. Conversely, there was an electrical delay attributed to the interruption of the primary current and the growth time of the secondary current for the CIS. This delay at high engine speeds suggests a potential weakness in the CIS. Therefore, it can be deduced that higher spark energy with LIS contributes to increased combustion efficiency, elevated engine power, and a flawless combustion process that minimizes environmental pollution. These properties highlight the advantages of using a LIS in the motorcycle.

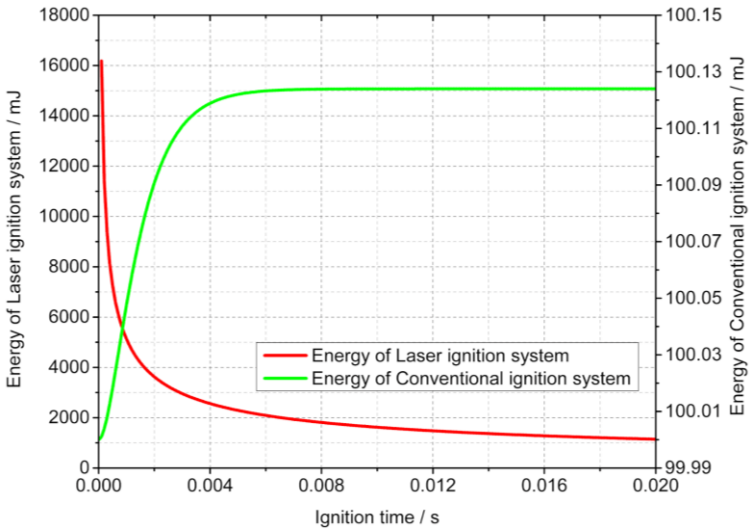

Figure 14. Energy of LIS and CIS in this study

3.3 Engine Power, Torque, and Specific Fuel Consumption between Using LIS and CIS

During engine operation, engine power, torque, and SFC play a crucial role in evaluating engine performance. Figure 15 illustrates the engine power comparison between the use of LIS and CIS in the Honda Future FI 125cc. It can be observed that when the speed of the engine increased, the engine power gradually increased and reached a maximum. Subsequently, the engine power gradually decreased due to engine instability and decrease in volume efficiency. Additionally, the mixture of air and fuel was not fully burned in the cylinder. This resulted in the residual mixture remaining in the cylinder, preventing the entry of fresh mixture into the chamber. Moreover, the curve shape of engine power was shown and found to be appropriate with theoretical predictions, as also presented and elucidated in [46].

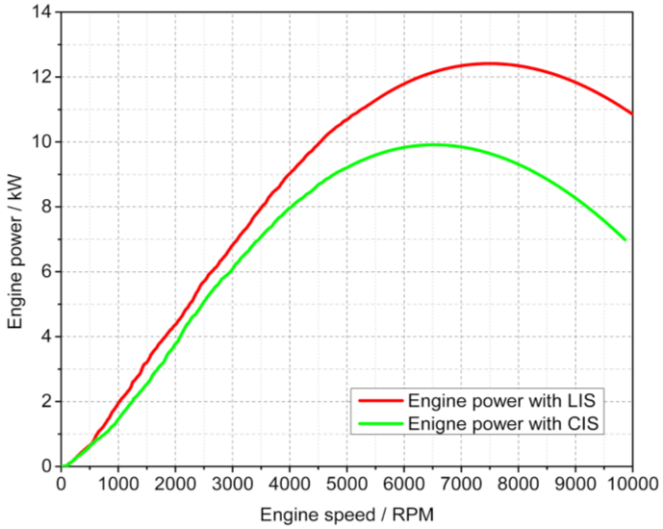

Figure 15. Engine power using LIS and CIS

At engine speeds lower than 500 RPM, the engine power was nearly the same for both LIS and CIS. This was because the energy of both LIS and CIS could be adapted at low engine speeds. However, when the engine speed exceeded 1000 RPM, the power of the engine with LIS surpassed that with CIS in the range of 1500 RPM to 4500 RPM. This occurred because the engine operation was optimal, and the intake and exhaust processes were optimized within this range of engine speed. Importantly, the energy of LIS was sufficiently high, resulting in complete combustion of the mixture. Therefore, the engine power with LIS was higher than the engine power with CIS. Beyond 4500 RPM up to 10000 RPM, there was a significant difference in engine power due to the higher efficiency of LIS compared to CIS. As the engine speed increased, CIS could not adapt due to the limited growth of secondary current at high engine speed, resulting in low energy. Meanwhile, the energy of LIS did not depend on the engine speed, as LIS could adapt to all ranges of engine speed. The misfire phenomenon did not occur in LIS due to the high laser energy required to burn the mixtures in the cylinder.

The engine power with LIS always responded to all engine operating modes because the technique of controlling the laser was much easier than that of the CIS. On the other hand, the energy of the laser was well-adapted and responded quickly with no lag phenomenon. In the CIS, the lag phenomenon occurred at high engine speeds due to the need for the growth of secondary current in the ignition coils and depended on the number of winding coils. Therefore, the ignition system was also one of the factors that affected the engine power.

The maximum engine power with CIS reached 10 kW at 6500 RPM. In contrast, the maximum engine power with LIS was reached with an expanded range, approximately 12.5 kW at 7500 RPM, because the entire air-fuel mixture was burned completely. Therefore, the chamber had fewer residual products after the burn, making it easier for the fresh mixture to enter the cylinder. The engine power reached its maximum, after which the engine power decreased due to loss of balance, increasing engine temperature, and friction matter. When the engine used LIS, the engine power increased by 1.25 times compared to the engine power with CIS, showing the superior features of the engine when using the LIS in the motorcycle.

Figure 16 shows the engine torque with LIS and CIS. The engine torque is a vital parameter in evaluating engine characteristics. Consequently, the engine torque curve exhibited a profile similar to the engine power curve. It was observed that the engine torque gradually increased, reaching a maximum, and then gradually decreased due to engine instability and a decrease in volume efficiency.

At engine speeds lower than 500 RPM, the engine torque with LIS and CIS gradually increased and had nearly the same value. However, when the engine speed exceeded 1000 RPM, there was a noticeable difference in engine torque between LIS and CIS. Specifically, the maximum engine torque with CIS reached approximately 9 N.m at 4200 RPM. In contrast, the maximum engine torque for the engine using LIS was attained at 10.5 N.m at 5000 RPM. The maximum torque of the engine with LIS was achieved with an expanded range of engine speed.

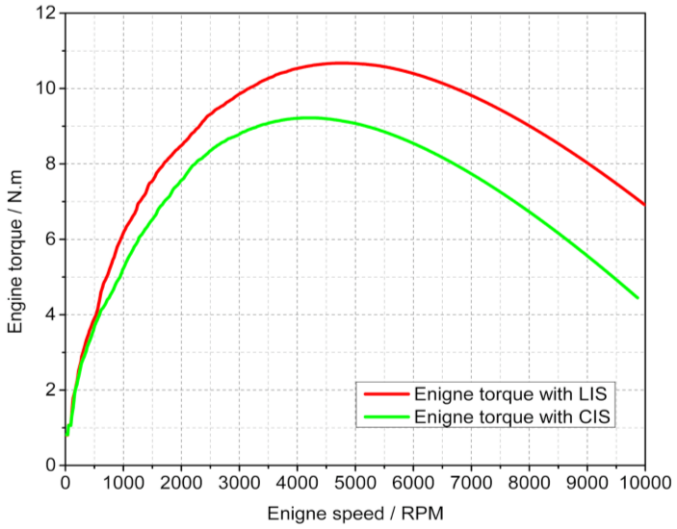

Figure 16. Engine torque with LIS and CIS

Specific fuel consumption (SFC) is a key parameter used to evaluate the economic characteristics that are related to the fuel efficiency of an engine in this study. According to the theory, a lower value of the SFC is better, indicating that the engine is achieving optimal fuel economy. After starting the engine, the SFC gradually decreased until it reached its lowest point. After that, the SFC gradually increased owing to fuel consumption for engine power following the theoretical model outlined in reference [47]. Figure 17 shows the comparison of SFC value between LIS and CIS in the Honda Future FI 125cc engine. The SFC was high during engine startup due to the prolonged operation of the fuel injector, which was aimed at enriching the mixture and resulting in increased fuel consumption. This phenomenon was observed at an engine idle speed of less than 500 RPM, where fuel consumption was high, and the SFC values for engines with LIS and CIS were identical. This similarity occurred because both LIS and CIS were adapted for the low engine speed range. However, at engine speeds over 1000 RPM, the SFC with CIS was higher than with LIS. This can be explained that the ignition efficiency of CIS was lower than the ignition of LIS when engine speed increased. At the range of engine speed of 1500 – 4500 RPM, the advantage of LIS over CIS became apparent. Notably, at engine speeds exceeding 6500 RPM, the SFC value increased for both the LIS and CIS due to less effective combustion in the chamber and a reduction in volumetric efficiency.

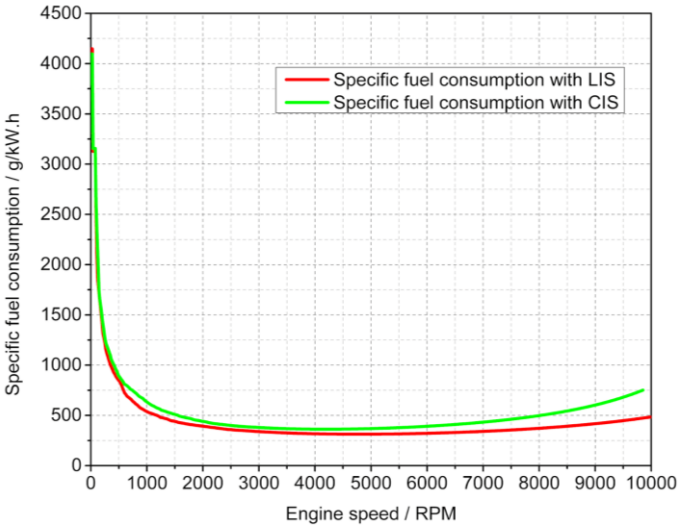

Figure 17. Specific Fuel Consumption for engines using LIS and CIS

However, the SFC with LIS is still lower than that with CIS because the energy of the laser could adapt to an extended range of engine speeds. On the other hand, LIS energy was not dependent on the growth of secondary current. Meanwhile, CIS energy could fail at high engine speeds, as it depended on interrupt current and the growth of secondary current, resulting in CIS energy not reaching high levels at high engine speeds. This could lead to engine misfires at high engine speeds, where the mixture could not be burned completely and remained in the chamber, resulting in a low air mass in the cylinder for CIS. Overall, the SFC with LIS was lower than the SFC with CIS across all engine speed ranges. Notably, the optimal SFC with CIS and LIS was achieved at engine speeds of 3470 and 4320 RPM, respectively. The optimal fuel efficiency of LIS was achieved with an extended range of engine speeds compared to the optimal fuel efficiency of CIS because the volumetric efficiency and combustion process with LIS in the cylinder were better than with CIS. On the

other hand, within this range of engine speeds, the LIS efficiency was higher than the CIS efficiency. The SFC with LIS was reduced by approximately 0.864 times compared to the SFC with CIS at the optimal engine speed within the range of 1500 – 4500 RPM.

In general, the engine performance was slightly identical value during engine operation at low speeds of 500 RPM for both the LIS and CIS. When the engine speed increased, the power and torque of the engine with LIS were superior to CIS. In contrast, the SFC with LIS was achieved lower than with CIS, indicating that using LIS saved fuel and emitted fewer pollutants into the environment.

3.4 Mass Fraction Burned (MFB) Comparison between Using LIS and CIS

The mass fraction burned (MFB) was a parameter utilized in combustion analysis to evaluate the effectiveness of the combustion process in the cylinder. MFB played a crucial role in understanding and optimizing combustion efficiency, emissions, and overall engine performance in internal combustion engines and other combustion systems. MFB represented the percentage of the fuel mass that had burned to the overall mass of fuel present in the chamber of combustion. In addition, it depended on the energy of ignition, meaning that if the energy of ignition was sufficient, the entire mixture of air and fuel would be burned.

Figure 18 shows the mass fraction burned with LIS and CIS under various engine speeds. The S-shaped curve of MFB closely resembled the theoretical predictions outlined in reference [48-49]. It was observed that the MFB with LIS and CIS gradually increased from 0 to 1.0 as the engine speed increased. The MFB with LIS consistently exceeded that with CIS. This can be explained by the more effective combustion of mixtures in LIS compared to CIS, attributed to the high effectiveness of the intake process, adaptability of LIS energy within the range of engine speed, and fast adaptive time. Consequently, the combustion quality of an engine is high when using LIS, with no residual gas left in the chamber, leading to a high charging efficiency.

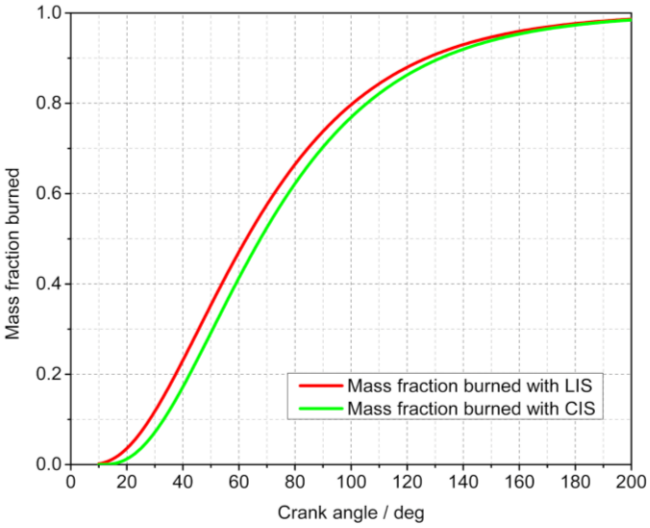

Figure 18. Mass Fraction Burned with LIS and CIS

4.0 CONCLUSIONS

In this study, a comparison of engine performance between LIS and CIS in the Honda Future FI 125cc engine was conducted through simulation, including the CFD and numerical simulation. Some conclusions were drawn as follows:

- The volumetric efficiency with LIS was better than that of CIS because residual combustion products were removed during engine operation. Therefore, the air mass in the cylinder with LIS was higher than with CIS.
- At low engine speed, the engine performance does not seem to be affected by both LIS and SIS. This was because both LIS and CIS were adapted for low engine speeds.
- The advantage of LIS over CIS becomes evident across all ranges of engine speeds. Additionally, engines utilizing LIS demonstrate higher performance, with the maximum engine performance achieved in an extended range of engine speeds compared to CIS.
- The fuel efficiency with LIS surpassed that of CIS, suggesting that utilizing LIS led to fuel savings and reduced emissions of pollutants into the environment. Consequently, the engine equipped with LIS proved to be more fuel-efficient and cost-effective.
- The efficiency of mass fraction burned with LIS was higher than with CIS. It can be observed the mixture of fuel and air was burned completely, leaving no residual gas in the chamber, which resulted in high charging efficiency.

Overall, the engine performance and fuel efficiency with LIS were better than with CIS in this study. This finding is significant for assessing the advantages of LIS in motorcycles, particularly in engines like the Honda Future FI 125cc.

Furthermore, this model can be used to evaluate engine performance between LIS and CIS in any motorcycle. This model establishes the theoretical foundation for the next study, which aims to validate the comparison between experimental and theoretical results.

5.0 ACKNOWLEDGEMENTS

During the implementation of this research, the National Chung Cheng University (NCCU) and Ho Chi Minh City University of Technology and Education (HCMUTE) were acknowledged for their financial support in this research.

6.0 REFERENCES

[1] Montenegro, Gianluca, et al. "Fluid dynamic and acoustic optimization methodology of a motorbike intake airbox using multilevel numerical CFD models and experimental validation tests," *SAE International Journal of Engines,* vol. 6, no. 3, pp. 1731-1744, 2013.

[2] Porter, Matt, "Intake manifold design using computational fluid dynamics," The UNSW Canberra at ADFA *Journal of Undergraduate Engineering Research,* vol.1, no.2, p. 31, 2009.

[3] Ly, Vinh Dat, Thanh Quang Le, and Tan Thich Do, "A study of the effects of swirl and tumble ratios on engine performance in motorbike," *Journal of Technical Education Science*, vol. 14, no.3, pp. 58-65, 2019.

[4] Subroto, Subroto, Sartono Putro, and Pramuko Ilmu Purboputro, "Experimental study of motorcycle performance with exhaust manifold using torque expansion chamber," *JTTM: Jurnal Terapan Teknik Mesin,* vol. 5, no. 1, pp. 46-53, 2024.

[5] Duy, Vinh Nguyen, et al. "Experimental study on improving performance and emission characteristics of used motorcycle fueled with ethanol by exhaust gas heating transfer system." *Energy for Sustainable Development,* vol. 51, pp. 56-62, 2019.

[6] Ilyas, Shahzaib, Usama Naveed, and Junaid Khalid, "Improving fuel consumption using Electronic Fuel Injection Technology for low-powered Motorbike Engine," 2020 *17th International Bhurban Conference on Applied Sciences and Technology (IBCAST)*. IEEE, 2020.

[7] Tong, Chia-Chang, and Wu-Shun Jwo, "An assist-mode hybrid electric motorcycle," *Journal of Power Sources,* vol. 174, no. 1, pp. 61-68, 2007.

[8] Iyer, Narayan V., Francisco Posada, and Anup Bandivadekar, "Technical assessment of emission and fuel consumption reduction potential from two and three-wheelers in India," No. 2013-26-0050. *SAE Technical Paper*, 2013.

[9] Miên, Trịnh Lương, and Trương Mạnh Hùng, "A New Method to Control Fuel-Saving Eco-Motorbike at the Competition "Honda 2018 Fuel-Saving Eco-Motorbike Driving," *International Journal of Engineering Research et Technology,* vol. 12, no. 7, pp. 977-985, 2019.

[10] Lackner, Maximilian, et al. "Laser ignition in internal combustion engines-a contribution to a sustainable environment," Institute of Chemical Engineering. *Vienna University of Technology, Getreidemarkt*, vol. *9*, p.166., 2004.

[11] M. McMillian, S. Richardson, S. D. Woodruff, and P. Tran, "Laser spark ignition for natural gas fuels reciprocating engines," in Proc. *Gas Machinery Conference* 2003, paper 2003–103, Gas Machinery Research Council, Dallas, TX 2003.

[12] Dodd, Robert, et al. "Laser ignition of an IC test engine using an Nd: YAG laser and the effect of key laser parameters on engine combustion performance," *Lasers in Engineering*, vol. 17, no. 3, pp. 1554-2971, 2007.

[13] McIntyre, Dustin L, "A laser spark plug ignition system for a stationary lean-burn natural gas reciprocating engine," PhD Thesis, West Virginia University, 2007.

[14] Phuoc, Tran X., and Fredrick P. White, "Laser-induced spark ignition of CH4/air mixtures," *Combustion and flame,* vol. 119, no. 3, pp. 203-216, 1999.

[15] El-Rabii, H., and J. C. Rolon, "Experimental study of laser ignition of a methane/air mixture by planar laser-induced fluorescence of OH," *Proc. PSFVIP*, pp. 1-4, 2003.

[16] Horisawa, Hideyuki, et al. "Effects of a focused laser pulse for combustion augmentation characteristics in supersonic airstreams," *Vacuum,* vol. 73, issues. 3-4, pp. 439-447, 2004.

[17] Spiglanin, T. A., et al. "Time-resolved imaging of flame kernels: laser spark ignition of H2/O2/Ar mixtures," *Combustion and Flame,* vol. 102, no. 3, pp. 310-328, 1995.

[18] McIntyre, Dustin L., et al. "Laser spark plug development," *SAE Transactions,* pp. 1101-1111, 2007.

[19] Mullett, J. D., et al. "Multi-cylinder laser and spark ignition in an IC gasoline automotive engine: a comparative study," No. 2008-01-0470. *SAE Technical Paper*, 2008.

[20] Syage, J. A., et al. "Dynamics of flame propagation using laser-induced spark initiation: Ignition energy measurements," *Journal of Applied Physics*, vol. 64, no. 3, pp. 1499-1507, 1988.

[21] Ryu, S. K., S. H. Won, and S. H. Chung, "Laser-induced multi-point ignition with a single-shot laser using conical cavities and prechamber with jet holes," *Proceedings of the Combustion Institute,* vol. 32, no. 2, pp. 3189-3196, 2009.

[22] Dale, J. D., P. R. Smy, and R. M. Clements, "Laser ignited internal combustion engine-an experimental study," *SAE Transactions,* pp. 1539-1548, 1978.

[23] Weinrotter, Martin, et al. "Laser ignition of ultra-lean methane/hydrogen/air mixtures at high temperature and pressure," *Experimental thermal and fluid science,* vol. 29, no. 5, pp. 569-577, 2005.

[24] Srivastava, Dhananjay Kumar, et al. "Characterisation of laser ignition in hydrogen-air mixtures in a combustion bomb," *International Journal of Hydrogen Energy*, vol. 34, no. 5, pp. 2475-2482, 2009.

[25] Kopecek, Herbert, et al. "Laser ignition of methane-air mixtures at high pressures and diagnostics," *Journal of Engineering for Gas Turbines Power*, vol. 127, no. 1, pp. 213-219, 2005.

[26] Zhai, Guanxiong, et al. "Laser ignition of iso-octane and n-heptane jets under compression-ignition conditions," *Fuel*, vol. 311, p. 122555, 2022.

[27] Endo T, Kuwamoto K, Kim W, Johzaki T, Shimokuri D, Namba S, et al. "Comparative study of laser ignition and spark-plug ignition in high-speed flows," *Combustion and Flame*, vol. 191, pp. 408-16, 2018.

[28] Patil, S. S., and M. R. Nandgaonkar, "Numerical analysis of gasoline fuel with laser ignited spark ignition," *Journal of Physics: Conference Series*, vol. 1240, no. 1, IOP Publishing, 2019.

[29] Mohamed H, "An experiment on the combustion characteristics with laser-induced spark ignition," *KSME International Journal*, vol. 13, pp. 82-89, 1999.

[30] Kopecek, Herbert, et al. "Laser ignition of methane-air mixtures at high pressures," *Experimental Thermal and Fluid Science*, vol. 27, no. 4, pp. 499-503, 2003.

[31] Wang, ChangJian, ShengLi Xu, and GuangMing Jia, "Laser-induced spark ignition of H_2/O_2/Ar mixtures," *Science in China Series E: Technological Sciences*, vol. 50, pp. 797-806, 2007.

[32] Zambalov, Sergey D., Igor A. Yakovlev, and Vladimir A. Skripnyak, "Numerical simulation of hydrogen combustion process in rotary engine with laser ignition system," *International Journal of Hydrogen Energy*, vol. 42, no. 27, pp. 17251-17259, 2017.

[33] Kopecek, Herbert, et al. "Laser-stimulated ignition in a homogeneous charge compression ignition engine, " *No. 2004-01-0937. SAE Technical Pape*r, 2004.

[34] Pal, Anuj, and Avinash Kumar Agarwal, "Effect of laser pulse energy on laser ignition of port fuel injected hydrogen engine," *International Journal of Hydrogen Energy*, vol. 41, no. 1, pp. 675-682, 2016.

[35] Kuang, Zheng, et al. "Multi-location laser ignition using a spatial light modulator towards improving automotive gasoline engine performance," *Optics and Lasers in Engineering*, vol. 90, pp. 275-283, 2017.

[36] Liedl, Gerhard, et al. "Laser-induced ignition of gasoline direct-injection engines," *XV International Symposium on Gas Flow, Chemical Lasers, and High-Power Lasers*, Vol. 5777, SPIE, 2005.

[37] McMillian, Michael H., et al. "Laser spark ignition: laser development and engine testing," *Paper Number ICEF2004-917, Proceedings of ICEF04 2004 Fall Technical Conference of the ASME Internal Combustion Engine Division*, 2004.

[38] Heywood, "Internal Combustion Engine Fundamental," *Gc Graw-Hill*, book, 1998.

[39] Assoc. Prof. Dr. Dzung Do Van, "Electrical ICE and Management Engine, " *Published at VNU*, book, 2013.

[40] Moskwa, John Joseph, "Automotive engine modeling for real-time control," *Diss. Massachusetts Institute of Technology*, 1988.

[41] Khan, N., N. Abas, and A. Kalair, "Multiline distributed feedback dye laser endorses Wien's displacement law," *Applied Physics B*, vol. 122, pp. 1-7, 2016.

[42] Yagi, Shizuo, et al. "Estimate of Total Engine Loss and Engine Output in Four Stroke SI Engines," *SAE transactions*, pp. 530-541, 1991.

[43] Colin, G., et al. "In-cylinder mass estimation using cylinder pressure," No. 2007-24-0049. *SAE Technical Paper Series, 8th International Conference on Engines for Automobiles*, 2007.

[44] Trawniczek, Franz, "Calculation and simulation of Q-switched laser ignition sources," *Diploma Thesis*, Vienna University of Technology, pp.56-67, 2009.

[45] Chehroudi, Bruce, "Laser ignition for combustion engines," *Advances Laser Applications Conference and Exposition*, 2004.

[46] Gupta, Hari N, "Fundamentals of internal combustion engines," *PHI Learning Pvt. Ltd*., pp. 533-535, book, 2012.

[47] Stone, Richard, "Introduction to internal combustion engines," vol. 3. *London: Macmillan*, pp. 116-118, book, 1999.

[48] Kirkpatrick, Allan T, "Internal combustion engines: applied thermosciences," *John Wiley & Sons*, pp. 58-60, book, 2020.

[49] Mittal, M., G. Zhu, and H. Schock, "Fast mass-fraction-burned calculation using the net pressure method for real-time applications," *Proceedings of the Institution of Mechanical Engineers, Part D: Journal of Automobile Engineering*, vol. 223, no. 3, pp. 389-394, 2009.

NOMENCLATURE

a	Effect coefficient on the combustion process	Q_{hr}	Heat release (J)
A_c	Combustion chamber area (m^2)	Q_{ht}	Heat transfer (J)
$A(\varphi)$	Function of throttle valve with crank angle (m^2)	Q_{HV}	Heating value of the fuel (MJ/kg)
b	Wien's displacement coefficient (m.K)	r	Crank radius of the engine (m)
C	Capacitive in the primary coils and secondary coils (F)	R	Universal gas constant (mol^{-1} K^{-1} J)
C_1	Primary coils capacitance (F)	R_1	Primary winding resistance (Ω)
C_2	Secondary coils capacitance (F)	R_L	Radius of the laser after passing the focal (m)
C_d	Coefficient of discharge	R_{st}	Summation of turbulent ratios (swirl and tumble ratio).
C_D	Coefficient of dimension	t_1	Ignition factor coefficient (H. Ω^{-1})
CFD	Computational Fluid Dynamics	t_d	Ignition time (ms)

CIS	Conventional Ignition System
C_r	Engine compression ratio
d_L	Laser beam diameter (mm)
d	Diameter of the throttle shaft (m)
D_P	Piston diameter (m)
D	Diameter of the throttle bore (m)
D_{in}	Diameter of intake manifold (m)
E_B	Threshold energy required to generate a laser
E_C	Ignition energy of capacitive (mJ)
E_{CIS}	Conventional ignition system energy (mJ)
E_I	Ignition energy of inductive (mJ)
E_{LIS}	Laser ignition system energy (mJ)
f	Focal length of the laser (mm)
h	Coefficient of convective heat transfer ($m^{-2}K^{-1}W$)
I_B	Threshold-breaking power density
I_{int}	Interrupt current in CIS (A)
k	Air's specific heats ratio
K_i	Ignition reserve coefficient
L	Connecting rod length (m)
L_1	Primary coils inductance (H)
L_i	Intake valve opening (mm)
L_e	Exhaust valve opening (mm)
LIS	Laser Ignition System
m	Effect coefficient on the combustion process
$\dot{m}_{ai}$	Upstream of air mass flow rate, before the throttle valve (g/s)
$\dot{m}_{ao}$	Downstream of air mass flow rate output, after passing the component of the throttle valve (g/s)
M_{ac}	Mass of air charged in cylinder (g)
m_f	Fuel mass per cycle
N	Engine speed (RPM)
N_V	Number of valves
RPM	Revolution Per Minute
P_0	Upstream pressure of air (bar)
P_{br}	Engine power output (W)
P_m	Pressure of the air at the intake manifold (bar)
P_L	Laser pulse power (kW)
P_p	Pumping loss (MPa/RPM^2)
P_t	Pressure of throat throttle at the minimum area of the throttle valve (bar)
t_L	Ignition time under laser beam (ms)
T	Temperature during charging (K)
T_0	Upstream temperature of the air (K)
T_{br}	Engine brake torque (N.m)
T_F	Function of torque (N.m/g)
T_{fr}	Friction torque of engine (N.m)
T_g	Mixture combustion temperature (K)
T_{ind}	Indicated engine torque (N.m)
T_m	Temperature of the air at the intake manifold (K)
T_w	Combustion wall temperature (K)
U_1	Primary winding potential (V)
U_2	Secondary winding potential (V)
V_d	Displacement volume (m^3)
V_L	Lubrication oil viscosity (Mpa)
x_b	Mass fraction burned

Greek letters

α	Throttle valve angle (deg)
α_0	Initial angle throttle valve (deg)
η_{CIS}	CIS ignition performance
η_v	Volumetric efficiency
λ	Laser wavelength (nm)
φ	Crankshaft angle (rad)
φ_0	Advanced ignition system (deg)
φ_d	Total of combustion time (s)
ω_e	Angular velocity of an engine (rad/s)

Superscripts and subscripts

ai	air in
ao	air out
d	discharge
e	engine
f	fuel
g	gas mixture
m	manifold
p	pumping